Acta Geodyn. Geomater., Vol. 22, No. 3 (219), 393–404, 2025
DOI: 10.13168/AGG.2025.0027
journal homepage: https://www.irsm.cas.cz/acta

ORIGINAL PAPER

AGRICULTURAL AND ENERGY SECTORS DOMINATE IRAN'S WATER CRISIS: A GRACE-GLDAS QUANTIFICATION (2002–2023)

Xilong YUAN [1], Yunqi ZHOU [2] *, Shijian ZHOU [3] and Fengwei WANG [4]

[1] *School of Surveying and Geoinformation Engineering, East China University of Technology, Nanchang 330013, China*
[2] *School of Geographical Sciences, University of Bristol, Bristol BS8 1SS, UK*
[3] *School of Software, Nanchang Hangkong University, Nanchang 330063, China*
[4] *College of Surveying and Geoinformatics, Tongji University, Shanghai, PR, China*

**Corresponding author's e-mail:* yunqi.zhou@bristol.ac.uk

ARTICLE INFO

Article history:
Received 10 April 2025
Accepted 29 August 2025
Available online 25 September 2025

Keywords:
Crustal anisotropy
Moho and Conrad discontinuities
Common Conversion Point (CCP) stacking
410 km and 660 km discontinuities
Receiver function
Southeast Asia tectonics

ABSTRACT

Iran faces a severe water security crisis characterized by chronic precipitation deficits and uneven freshwater distribution, with >80 % of surface water concentrated in northern/northwestern basins. This hydrological stress is exacerbated by anthropogenic activities, particularly in regions such as the western Tehran Plain, where groundwater extraction exceeds the natural recharge capacity by 150 %, rendering 72 % of monitored aquifers critically vulnerable (<10 % of the safe yield threshold). In this study, a comprehensive analysis of Terrestrial Water Storage (TWS) changes in Iran (April 2002–December 2023) was conducted, integrating multisource GRACE mascon solutions (JPL, CSR, and GSFC) with the GLDAS-Noah hydrological model. Missing GRACE data (excluding the July 2017–May 2018 gap) were interpolated using cubic splines. The results reveal a distinct shift in the TWSC trend. Prior to 2007, the TWSC was relatively stable (linear trend: 0.12 ± 0.13 cm/yr); after 2007, the TWSC rapidly declined (linear trend: -0.52 ± 0.03 cm/yr), which was primarily driven by anthropogenic groundwater extraction for the energy and agricultural sectors. Spatial analysis revealed moderate rates of decrease in the southwest (46°–52°E, 28°–34°N; -0.32 cm/yr) and northeast (56°–60°E, 38°–39°N; -0.28 cm/yr), whereas other regions exhibited severe depletion. In particular, acute anthropogenic overexploitation was observed in the southern piedmont of the Alborz Mountains (48°–52°E, 34°–37°N), where the TWSC decreased at rates exceeding 20 cm/yr, with the most severe depletion occurring in the western Tehran Plain (51.2°–51.5°E, 35.5°–35.7°N). Localized decreases surpassing 10 cm/yr characterized the Rafsanjan Basin (54°–59°E, 29°–31°N). Anthropogenic factors accounted for 77 % of the combined groundwater–surface water losses after oil extraction impacts were excluded. The transfer of irrigation-induced groundwater to surface systems, which was subsequently lost via evapotranspiration, constituted 64 % of the TWSC loss. Our integrated approach–synthesizing multisource GRACE solutions with GLDAS modeling–establishes a transferable framework for monitoring climate–human interactions in arid-region hydrology.

1. INTRODUCTION

Freshwater resources are fundamental to societal functioning and ecosystem integrity. Quantifying terrestrial water storage (TWS) dynamics enables the assessment of regional water availability, informing evidence-based allocation policies and sustainable water cycle management. Changes in the TWS of a region directly affect agricultural irrigation and the health of ecosystems. However, global groundwater depletion has accelerated since 2000 (Bhattarai et al., 2021). This depletion is driven by unsustainable extraction and climate-mediated stressors, notably, rising temperatures that increase evapotranspiration and reduce recharge. This depletion threatens agricultural resilience and ecosystem health while triggering secondary hazards: land subsidence, seawater intrusion, and permanent aquifer compaction (Ehsan et al., 2024). Iran, which suffered severe TWS losses of 143.6 km³ during 2003–2009, epitomizes this crisis (Voss et al., 2013). In the Central Plateau Basin, groundwater storage has decreased 11.55 mm/yr (in equivalent water height) because of unsustainable extraction (Safdari et al., 2022a).

Traditional groundwater monitoring relies on in situ observation wells. However, this approach demands substantial resources (Safdari et al., 2022a; Ma et al., 2021) and suffers from human, instrumental, and spatial sampling errors, resulting in significant inaccuracies and constrained spatial resolution (Akhtar et al., 2022). Furthermore, the assessment of regional groundwater storage (GWS) changes requires a dense well network across the entire area. Although numerous spatial interpolation techniques have been developed to generate denser spatial maps of groundwater levels—such as relative area-based weighting within Thiessen polygons (Safdari et al., 2022b) or data-driven sparse sampling optimization (Ohmer et al., 2022) - these methods cannot inherently mitigate observational errors or increase data accuracy.

Cite this article as: Yuan X, Zhou Y, Zhou S, Wang F: Agricultural and energy sectors dominate Iran's water crisis: A GRACE-GLDAS quantification (2002–2023). Acta Geodyn. Geomater., 22, No. 3 (219), 393–404, 2025. DOI: 10.13168/AGG.2025.0027

In April 2002, the Gravity Recovery and Climate Experiment (GRACE) satellite mission was jointly launched by NASA and the German Aerospace Center (DLR). The satellites ceased operations in June 2017 and were replaced by GRACE-Follow On (GRACE-FO) in May 2018 (Wang et al., 2023). Although crustal movements (e.g., volcanic/seismic activity) perturb GRACE-derived water storage signals (Sun et al., 2024), short-term variations in Earth's gravity field predominantly reflect water mass changes, including changes in groundwater, soil moisture, glaciers/ice sheets, surface water, snowpack, and canopy storage (Eamus et al., 2015). GRACE detects global gravity anomalies that are converted to monthly TWS changes (Su et al., 2020). It can be used to recover changes in TWS over scales of hundreds of kilometers or larger, with a precision of less than 2 cm after processing (Tu et al., 2012). GRACE data are widely used to quantify groundwater storage anomalies (GWSA) across multiple scales (Liu et al., 2022; McStraw et al., 2022). For example, in North America, GRACE revealed groundwater depletion in the Mississippi River Basin (Xiao et al., 2015); in arid zones (e.g., Northwestern China), it was used to quantify groundwater storage dynamics and drought impact (Cao et al., 2015; Hosseini-Moghari et al., 2020); and in the Himalayas, it was used to measure glacier mass loss contributions to sea-level rise (Wang et al., 2017). Building on this global legacy, in this study, GRACE/GRACE-FO data is leveraged to investigate anthropogenic groundwater depletion in Iran.

Numerous studies have documented groundwater depletion across the Middle East, particularly in Iran. In 2020, Panahi et al. analyzed the changes in water resources in Iran over recent decades, including decreases in precipitation and runoff and increases in evapotranspiration (Panahi et al., 2020). In 2022, Azar et al. used synthetic aperture radar (SAR) to reveal groundwater extraction-induced surface subsidence and related disasters in regions such as the Hashtgerd Plain, Kerman Basin, and Alborz Basin in Iran (Azar et al., 2022). Additionally, Zaki et al. analyzed the impact of agricultural water use on water resource consumption in Iran (Zaki et al., 2020). These studies all concluded that the water resource situation in Iran is concerning, with many areas facing water shortages. To address Iran's increasing water stress and conventional monitoring constraints, we integrate multisource GRACE mascon solutions (JPL, CSR, and GSFC) with the GLDAS-Noah hydrological model (Yeh et al., 2006). This framework investigates spatiotemporal TWS change dynamics across Iran (2002–2023) and elucidates the underlying drivers. We reconstruct gap-filled TWSC time series via cubic spline interpolation (Pelliccia et al., 2020), quantify climate versus anthropogenic contributions to the TWSC, and identify pivotal trend shifts to assess human interventions. By fusing multi-institution GRACE solutions and hydrological models at the national scale, we develop a robust methodology for TWS analysis in arid regions. We performed segmented linear trend (Boshnakov, 2016) analysis on TWSC. Crucially, we excluded the influence of energy sector petroleum extraction from anthropogenic impact calculations, enabling more precise quantification of other human-driven factors affecting TWSC. Furthermore, spatial analysis revealed localized recharge mechanisms (Zagros Mountain runoff and Caspian Sea moisture influx), offering new data-driven insights for resilient water resource management strategies in Iran.

2. DATASETS AND STUDY REGIONS

2.1. DATASETS

2.1.1. GRACE DATA

This study utilizes the Release 06 (RL06) Mascon solutions from the Center for Space Research at the University of Texas at Austin (CSR), NASA's Jet Propulsion Laboratory (JPL), and NASA's Goddard Space Flight Center (GSFC). The dataset includes observations from both the GRACE mission and the successor mission, GRACE-FO. The JPL and GSFC mascon products feature a spatial resolution of 0.5°, whereas the CSR mascon data are provided at a higher resolution of 0.25°. To harmonize the spatial scales, the 0.25° CSR data were downsampled to a 0.5° global grid (720 × 360 cells) by computing the mean value within each target grid cell. These mascon solutions offer increased spatial resolution, effectively mitigate striping errors (Sun et al., 2018), add a degree-1 term, and replace the C_{20} coefficient. Adjustments for the glacial isostatic adjustment (GIA) effect were applied on the basis of the ICE6G_D model (Loomis et al., 2020). The study period spans from April 2002 to December 2023. During this period, data are unavailable for a total of 33 months. A primary gap of 11 months occurred between July 2017 and May 2018 because of the operational gap between the GRACE and GRACE-FO missions. For the remaining 22 months of missing data, values were estimated using cubic spline interpolation (Zhang et al., 2024).

2.1.2. HYDROLOGICAL DATA

In this study, the GLDAS-Noah hydrological model, a global medium-resolution offline land surface modeling system jointly developed by the Goddard Space Flight Center (GSFC) and the National Centers for Environmental Prediction (NCEP) (Shi et al., 2022), was utilized. This system features a spatial resolution of 0.5° and a temporal resolution of one month. The GLDAS-Noah data used in this study covered the period from April 2002 to December 2023 and were temporally consistent with the GRACE data. Compared with other GLDAS models, Noah demonstrates reduced bias and uncertainty in simulating water storage variations (Di Long et al., 2017). To quantify anthropogenic influences, we integrated precipitation, evapotranspiration, and runoff data from GLDAS-Noah with GRACE-derived

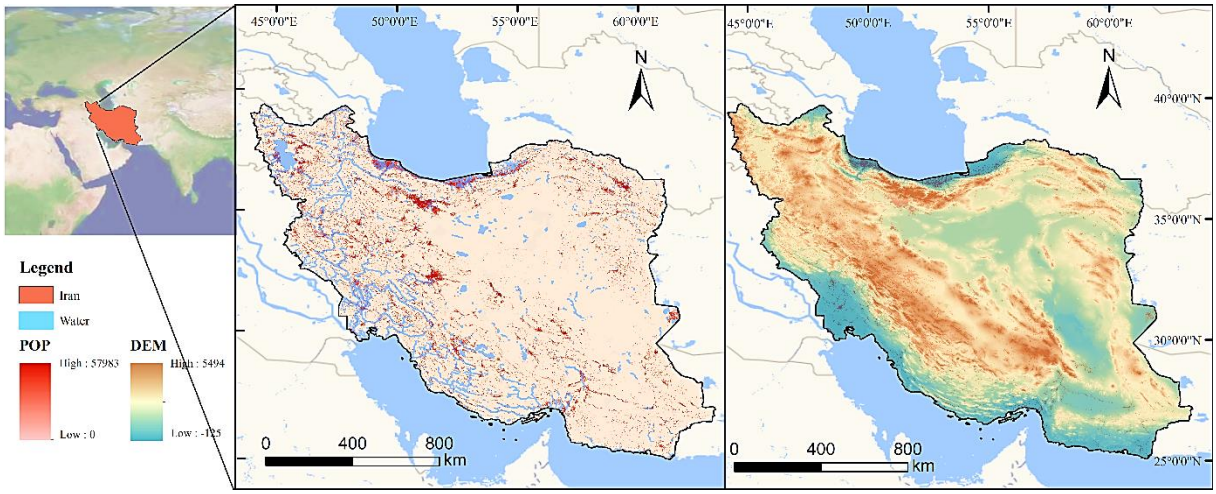

Fig. 1 Location map of the study area. Left: population distribution and river network as of 2023; Right: DEM.

TWSC estimates. Additionally, soil water storage, snow water equivalent, and canopy water storage from GLDAS-Noah were combined with GRACE observations to isolate surface water and groundwater components. Given Iran's location in the Middle East, where glacial coverage is negligible, glacial contributions to TWS were excluded from this analysis. Groundwater net extraction rates were sourced from the WaterGAP Global Hydrology Model (WGHM), which has a spatial resolution of 0.5° and monthly temporal resolution. The WGHM dataset covers April 2002 to December 2019. This model has been widely applied globally for water resource assessment and management applications (Hasan et al., 2025; Schmied et al., 2024).

2.1.3. OIL EXTRACTION DATA

In this study, annual crude oil production data from the Organization of Petroleum Exporting Countries (OPEC) annual reports is employed; these reports document member states' petroleum outputs, economic indicators, and global market dynamics. Specifically, Iran's annual oil production volume (2002–2023), which are reported each October in OPEC publications, served as the primary metric for evaluating country-scale extraction intensity.

2.2. STUDY REGION

The Islamic Republic of Iran (Iran), shown in Figure 1, is situated in Southwest Asia at the junction of Western and Central Asia. It extends from 44°E to 64°E longitude and 24°N to 40°N latitude, with an area of 1.64 million km². Iran's geomorphology is tectonically controlled by the Zagros Fold-Thrust Belt, which forms northwest–southeast mountain ranges that create sharp climatic gradients, including humid temperate zones in the Caspian highlands, hyperarid deserts in the central region, and hot–humid coasts along the Persian Gulf. Hydrologically, >70 % of surface runoff is derived from 25 % of the western mountains (Saedi et al., 2022), while groundwater supports 55 % of agriculture (Mirzaei et al., 2019) and accounts for 92 % of total freshwater consumption. The population distribution, river networks, and digital elevation model (DEM) of Iran are illustrated in Figure 1. Furthermore, as the holder of the world's fourth-largest oil reserves, Iran's petroleum extraction requires 3.1 billion m³/yr of water for well injection (e.g., for improved oil recovery), thereby intensifying aquifer depletion and triggering land subsidence exceeding 25 cm/yr in critical basins such as Isfahan (Lakhote et al., 2023).

3. METHODOLOGY

GRACE observations detect global terrestrial water mass changes. The processing workflow for Mascon RL06 products included (1) removal of the background gravity field at each grid cell using the January 2004–December 2009 mean period (selected as the reference baseline because of its established stability and widespread adoption in GRACE studies, representing a climatologically representative epoch with minimal large-scale hydroclimatic anomalies) as a reference, (2) spatial averaging of CSR Mascon data to achieve resolution parity with JPL and GSFC products, (3) computation of the ensemble mean across all three Mascon solutions as the terrestrial water storage change (TWSC) signal, and (4) gap-filling beyond July 2017–May 2018 using cubic spline interpolation to ensure temporal continuity. Separately, GLDAS-Noah simulates terrestrial water storage changes globally via the land water balance equation:

$$TWSC = \sum_{t=1}^{n} P_t - ET_t - RO_t + Q_t \quad (1)$$

where t denotes the monthly time index, P denotes total precipitation, ET denotes evapotranspiration, RO denotes runoff (including surface runoff and groundwater runoff), and Q denotes anthropogenic influences.

In Iran, Q_t primarily includes water consumption for petroleum extraction and agricultural irrigation. Background fields for P, ET, and RO were computed as their respective 2004.1–2009.12 temporal means. These background fields were subtracted from the original data on a per-grid-cell basis, which is consistent with Mascon processing. The natural water storage change computed through the GLDAS was formulated as follows (Wang et al., 2021):

$$TWSC_{GLDAS} = \sum_{t=1}^{n} P_t - ET_t - RO_t \quad (2)$$

Anthropogenic influences were quantified as follows:

$$\sum_{t=1}^{n} Q_t = TWSC - TWSC_{GLDAS} \quad (3)$$

Equation (3) quantifies anthropogenic contributions to terrestrial water storage by subtracting natural hydrological signals ($TWSC_{GLDAS}$) from GRACE-observed $TWSC$ signals. Critically, the characteristic rates of natural water storage changes (e.g., soil moisture, snowpack, and groundwater recharge) are substantially lower than the monthly mass variations resolved by GRACE. This rate disparity implies that the residual signal is predominantly controlled by anthropogenic activities—including petroleum extraction and its associated water consumption—which significantly alter regional mass budgets. To extract these components, we implement least-squares fitting using MATLAB with a parametric model consisting of one linear trend term and two cosine functions:

$$f = a + bt + A_1 \cos(\omega_1 t + \varphi_1) + A_1(\sin \omega_2 t + \\ + \varphi_2) + \varepsilon \quad (4)$$

where f represents the TWSC of the study area, $a + bt$ is the linear trend component, $A_1 \cos(\omega_1 t + \varphi_1)$ represents the annual signal, $A_1(\sin \omega_2 t + \varphi_2)$ represents the semiannual signal, and ε is the residual component.

All reported confidence intervals correspond to the 95 % level (equivalent to ±2 standard errors). This specific confidence level was computed under the fundamental assumption of Gaussian-distributed residuals. For each estimated parameter, the interval was calculated as the point estimate ± 2 × standard error, where the standard error quantifies the statistical uncertainty derived from the covariance matrix of the least-squares solution, scaled by the residual variance

After estimating anthropogenic influences and their linear trends using Equations (3) and (4), we focused on two major contributors to mass depletion in Iran: petroleum extraction and agricultural irrigation. To isolate the specific impact of agricultural water use, mass losses related to petroleum extraction and its associated water consumption were excluded. This approach is justified by the need to quantify and remove known nonagricultural influences, thereby enabling a clearer attribution of the remaining trend to irrigation. The net mass loss due to petroleum extraction was quantified using a water consumption-to-extraction ratio of 4:1, as reported in the International Journal of Health Sciences for 2004–2020, and total petroleum production data from OPEC. The total anthropogenic influence derived from Equation (3) was then adjusted by subtracting this petroleum-related mass loss. The residual trend was interpreted as being predominantly driven by agricultural water use. This conclusion is strongly supported by our quantitative analysis, which attributed approximately 7.2 % of the total depletion to petroleum activities, whereas the dominant remaining portion aligned with irrigation as the primary driver. According to the Catalogue of Hydrologic Analysis for Asia and the Pacific, Iran's total annual water consumption is approximately 9.8 billion m³, with 55 % derived from groundwater and agriculture accounting for 89 % of total withdrawals, confirming that irrigation is the dominant sectoral consumer. Net groundwater abstraction was estimated using the WGHM. The residual component, representing anthropogenic effects on surface water, was attributed primarily to the transfer of irrigation water to the surface, which is subsequently lost through evapotranspiration and runoff.

To quantify the relative contributions of anthropogenic groundwater impacts and surface water impacts to combined groundwater/surface water depletion, mass changes in these compartments were assessed by decomposing the TWSC into six components (Yang et al., 2021): surface water (SW), groundwater (GW), soil moisture (SM), snow water equivalent (SWE), canopy water (CW), and glaciers. The SM, SWE, and CW components were directly obtained from GLDAS-Noah. Given Iran's arid climate and negligible glacial coverage, glacial contributions were excluded. The residual mass variation after ΔSM, ΔSWE, and ΔCW are removed from the TWSC represents combined groundwater and surface water changes, as formalized in Equation (5).

$$\triangle TWS = \triangle SW + \triangle GW + \triangle SM + \triangle SnW + \\ + \triangle CW + \triangle Glacier \quad (5)$$

The soil moisture, snow water equivalent, and canopy water components were directly obtained from the GLDAS hydrological model. Thus, the residual component after subtracting soil moisture, snow water equivalent, and canopy water changes from GRACE observations represents groundwater variations below 200 cm depth and surface water changes encompassing reservoirs, rivers, and lakes.

4. RESULTS AND ANALYSIS

4.1. VALIDATION OF CHANGES IN TERRESTRIAL WATER STORAGE

Figure 2 contrasts the latitude-weighted TWSC time series derived from GRACE/GRACE-FO and its linear trend with the cumulative values from the latitude-weighted averaging of Equation (2) - based $TWSC_{GLDAS}$ sequences and its linear trends.

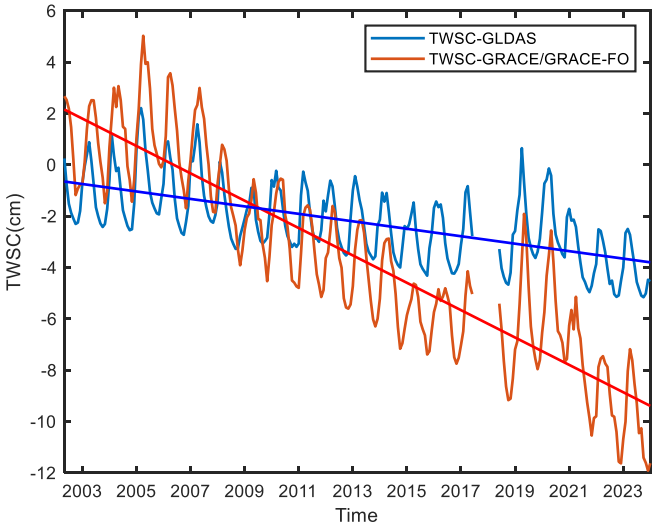

Fig. 2 The TWSC series estimated by the GRACE/GRACE-FO mascon and GLDAS models. For consistency with the GRACE/GRACE-FO observations, the same missing month data were deleted from the GLDAS model during the study period.

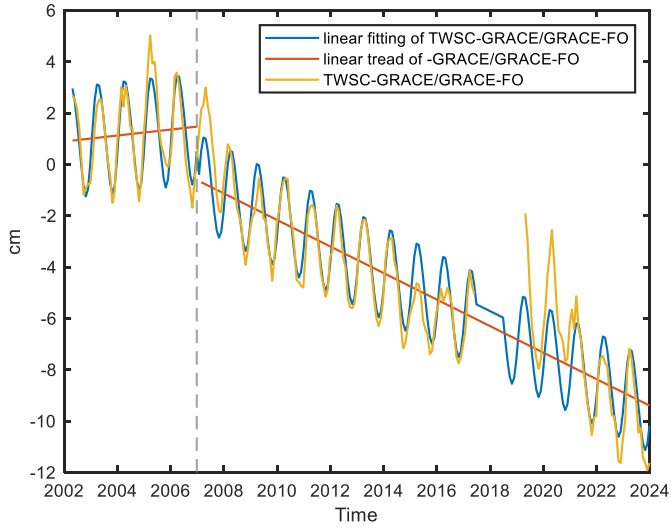

Fig. 3 Linear trend and least-squares fitted series of $TWSC$ for 2002.4–2006.12 and 2007.1–2023.12.

The two temporal series demonstrate marked concordance in their variational trends, exhibiting synchronized phase characteristics throughout the observation period. After the correlation analysis, the time lag effect was determined to be one month, with a correlation coefficient of 0.87, indicating that the GLDAS-Noah hydrological model provides a reliable estimate of surface water cycles and storage changes. For the period from April 2002 to December 2006, the estimated TWSC derived from the mascon and GLDAS models tends to increase; however, it tends to decrease for the period from January 2007 to December 2023.

4.2. ANALYSIS OF TWSC IN IRAN

4.2.1. TEMPORAL ANALYSIS

The $TWSC$ and $TWSC_{GLDAS}$ time series in Figure 2 show an increasing trend from 2002.4–2006.12, followed by a rapid decrease from 2007.1 to 2023.12. Accordingly, the $TWSC$ series was partitioned into these two temporal intervals for separate calculations of linear trends and least-squares fitted series (linear trends plus annual/semiannual signals), with the results shown in Figure 3.

The linear trend, annual amplitude, and semiannual amplitude are reported at the 95 % confidence level. After 2007.1, the terrestrial water storage variations in Iran demonstrated a reduced semiannual amplitude, indicating weakened hydrological oscillations at the semiannual scale. This phenomenon is correlated with groundwater overexploitation, where anthropogenic impacts have driven rapid depletion of groundwater reserves. Consequently, groundwater level fluctuations became constrained within semiannual cycles without pronounced variability. Over the 17-year period

Table 1 Linear trend and annual and semiannual amplitudes with uncertainties (95 % confidence intervals) of the $TWSC$ series during 2002.4–2023.12, 2002.4–2006.12 and 2007.1–2023.12.

Time	Linear trend [cm/yr]	Annual amplitude [cm]	Semiannual amplitude[cm]
2002.4-2023.12	-0.53±0.02	1.77±0.19	0.13±0.19
2002.4-2006.12	0.12±0.13	2.14±0.26	0.22±0.26
2007.1-2023.12	-0.52±0.03	1.81±0.20	0.26±0.20

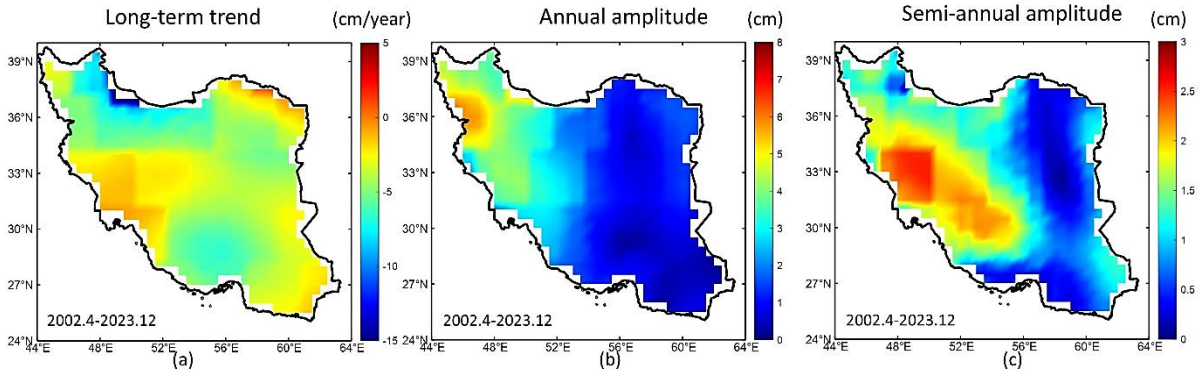

Fig. 4 (a) Spatial distribution of the linear trend in Iran; (b) spatial distribution of the annual cycle amplitude in Iran; (c) spatial distribution of the semiannual cycle amplitude in Iran.

(2007.1–2023.12), the TWSC significantly decreased linearly, which is consistent with extensive scientific consensus. This pattern is mechanistically driven by three interconnected factors: shifting precipitation regimes that reduce natural recharge, persistent groundwater over-extraction documented through monitoring wells (Safdari et al., 2022c), and intensive petroleum extraction activities that alter subsurface hydrology (Shami and Ghorbani, 2019).

4.2.2. SPATIAL ANALYSIS OF TWSC TRENDS

Spatial distribution maps of the linear trend of the TWSC (a), annual cycle amplitude of the TWSC (b), and semiannual cycle amplitude of the TWSC (c) of water resources in Iran from 2002.4 to 2023.12 are shown in Figure 4. The TWSC linear trend is relatively moderate in southwestern (46°-52°E, 28°-34°N) and northeastern (56°-60°E, 34°-37°N) regions (Fig. 4a). Northern areas (49°-51°E, 36°-38°N) exhibit accelerated decreases, with localized decreases exceeding -14 cm/yr (Fig. 4a). The annual cycle amplitudes are significantly greater in the northwestern region (45°-47°E, 35°-37°N) (Fig. 4b). The semiannual amplitudes remain relatively small overall (Fig. 4c), although values exceeding 2.5 cm occur in northwestern areas (47°-51°E, 31°-34°N) (Fig. 4c).

In the northern region of Iran (49°-51°E, 36°-38°N), accelerated TWSC depletion (> -14 cm/yr linear trend) coincides with pronounced annual amplitude fluctuations and diminished semiannual responses. This configuration signifies critical groundwater stress where seasonal recharge fails to offset intensive anthropogenic discharge. These findings are consistent with existing conclusions (Taheri et al., 2020) and suggest that more effective measures are needed to address the crisis. In the western region (46°-49°E, 31°-34°N), the relatively small annual cycle amplitude suggests muted seasonal precipitation–drought variability, whereas the increased semiannual amplitude implies significant intra-annual hydrological pulsing. Coupled with a stable linear trend and a slower depletion rate, this pattern signifies improved inherent hydrological resilience, buffering climate-driven stresses. Because the TWSC time series shows a gradual increase from 2002.4 to 2006.12 and a downward trend from 2007.1 to 2023.12, the GRACE data are divided into these two time periods. The linear trend, annual amplitude, and semiannual amplitude for the period from 2002.4 to 2006.12 are shown in Figure 5, whereas those for the period from 2007.1–2023.12 are shown in Figure 6.

From 2002.4–2006.12, the linear trend (Fig. 5a) in the southwestern region (46–52°E, 28–34°N) and northeastern region (56–60°E, 34–37°N) increased, with some areas experiencing an increase of more than 5 cm/year. These increases correspond to the areas with relatively mild decreases from 2002.4–2023.12 (Fig. 4a), suggesting that these two regions are more stable than others. The western region (44–49°E, 31–39°N) has significantly greater annual amplitudes (Fig. 5b). Compared with the period from 2002.4–2023.12 (Fig. 4c), the semiannual amplitude (Fig. 5c) was greater.

The spatial distribution of linear trends (Fig. 6a) from 2007.1–2023.12 aligns with patterns observed during the 2002.4–2023.12 (Fig. 4a) period. However, significant attenuation of annual (Fig. 6b) and semiannual amplitudes (Fig. 6c) occurred in the eastern (44–52°E) and northern regions (34–38°N) compared with the 2002.4–2006.12 (Fig. 5b, Fig. 5c) interval. This dampening primarily resulted from a post-2008 streamflow reduction, which decreased the seasonal hydrological variability. The decrease in

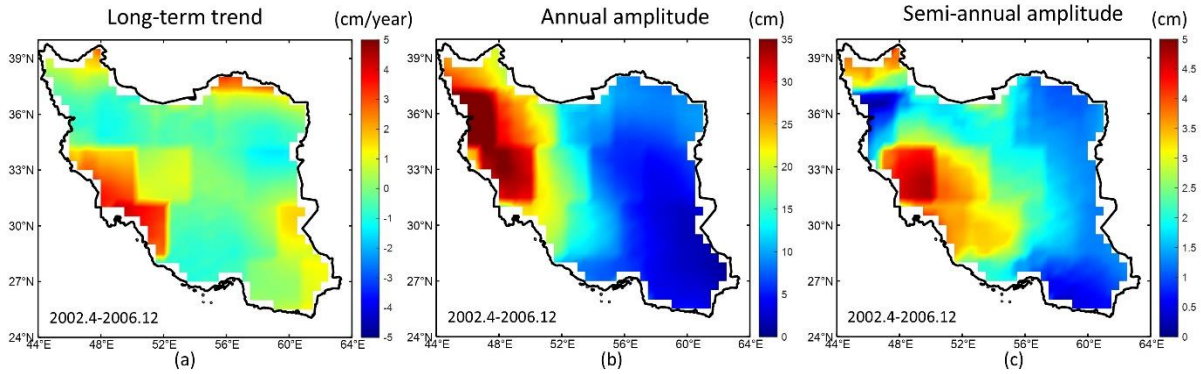

Fig. 5 Spatial distributions of TWSC in terms of (a) linear trend, (b) annual amplitude, and (c) semiannual amplitude over the period from 2002.4–2006.12.

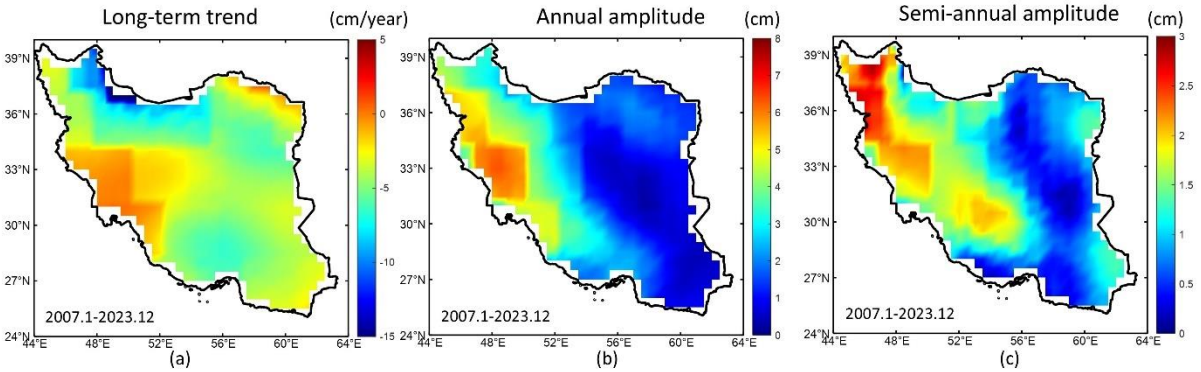

Fig. 6 Spatial distributions of TWSC in terms of (a) linear trend, (b) annual amplitude, and (c) semiannual amplitude for the period from 2007.1–2023.12.

streamflow strongly correlated with intensive groundwater exploitation, as evidenced by extreme TWS depletion and associated land subsidence: in the southern Alborz Mountains foothills (48–52°E, 34–37°N), the TWS linear trend exceeded -20 cm/yr, as indicated by a subsidence >16 cm/yr, and the Tehran Plain western sector (51.2–51.5°E, 35.5–35.7°N) experienced extreme subsidence rates exceeding 25 cm/yr (Haghighi and Motagh, 2019); the Rafsanjan Basin (54–59°E, 29–31°N) experienced a localized TWS linear decrease that surpassed -8 cm/yr, which was concurrent with land subsidence rates exceeding 20 cm/yr in the most affected aquifers. This differential response reflects aquifer-system compaction, where groundwater overextraction exceeds 150 % of the natural recharge capacity, resulting in an average annual volumetric storage loss of approximately 300 million cubic meters due to persistent overdraft (Motagh et al., 2017).

4.3. ANTHROPOGENIC IMPACTS ON TWSC

Natural water resource variations in Iran can be derived from Equation (3), whereby anthropogenic contributions to water storage changes are isolated by subtracting the natural component from the TWSC. Iran is a leading global petroleum supplier, and its energy sector—particularly its oil extraction and processing operations—constitutes a distinct anthropogenic water depletion component. Given the negligible magnitudes of glacial melt and coal mining in Iran, these nonhydrological contributions were excluded, allowing focused quantification of petroleum extraction impacts. Utilizing a documented petroleum extraction water-to-oil ratio of 4:1 barrel (International Journal of Health Sciences, 2004–2020), we quantified Iran's anthropogenic water depletion by integrating OPEC daily oil production data (2004.10–2023.10). Both the cumulative anthropogenic water depletion and the total mass depletion from petroleum extraction—converted to the equivalent water height (EWH) and encompassing the extraction of oil and the extraction of water for oil are shown in Figure 7.

As illustrated in Figure 7, the total mass depletion induced by petroleum extraction (blue curve) corresponds to the net mass loss, which encompasses both the direct mass reduction due to hydrocarbon extraction itself and the permanent outflow from the terrestrial water cycle. This outflow occurs through evaporative losses during drilling and flooding operations, contaminated water disposal, and water embedded in the extracted hydrocarbons. This loss is irreversible and accounts for 7.2 % of the total TWSC depletion in the study region of Iran, which is consistent with conclusions from existing studies. However, quantifying the precise contributions of petroleum extraction to TWSC is a highly complex and intricate task. During oil extraction, a large

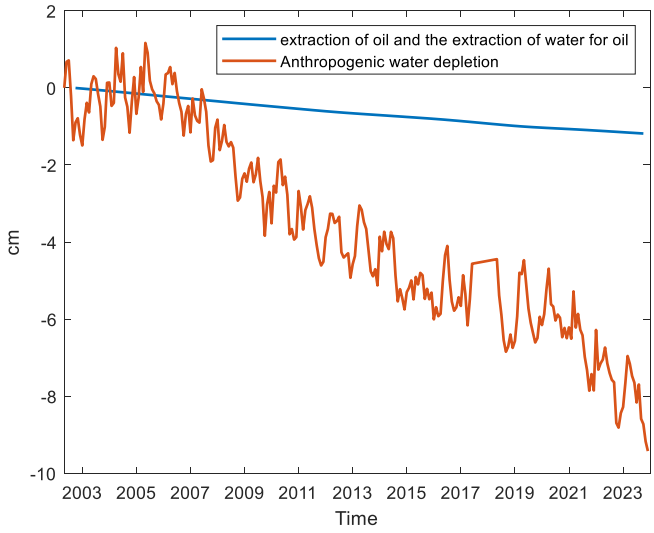

Fig. 7 The depletion of water resources due to the extraction of oil, the extraction of water for oil and anthropogenic water depletion.

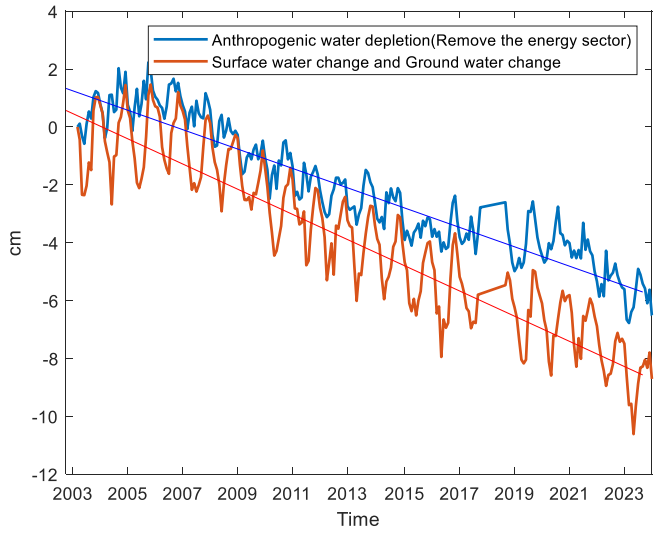

Fig. 8 Anthropogenic water consumption data (postsubtraction of energy sector water consumption) and surface water/groundwater data (postsubtraction of energy sector water consumption).

amount of liquid is extracted, leading to changes in geological structures and fault density (Khan et al., 2021) . Additionally, surface subsidence caused by reservoir depletion and compaction of sediment layers, as well as the extraction of fluids and drilling processes, can alter pore pressure, which triggers nontectonic seismic and other events. These activities contribute to the decrease in groundwater levels (Metois et al., 2020). When the oil extraction rate in a region slows, groundwater levels tend to recover as underground water pressure gradually stabilizes, and the reduction in pumping activity allows for some groundwater recharge (Luan et al., 2016). The rate of this recovery is influenced by factors such as precipitation, local conditions, and surface water. Concurrently, anthropogenic factors, including urbanization (Aslam et al., 2022) (e.g., the conversion of agricultural land to urban areas), deforestation (Ellison et al., 2024), and dam impoundment/discharge operations, have spatially heterogeneous effects on TWSC sequences, with the magnitudes of their influence varying across temporal and spatial scales.

Figure 8 contrasts surface and groundwater variations and their linear trends computed via Equation (5), with net anthropogenic impacts (excluding energy-sector consumption) and corresponding linear trends.

The strong correlation coefficient (0.94) between anthropogenic drivers and surface water/groundwater dynamics in Iran shown in Figure 8 indicates that anthropogenic activities dominate regional water resource depletion. Furthermore, both time series are strongly consistent with the TWSC trends, with accelerated declines observed after 2007. As quantified in Table 2, the anthropogenic contribution

Table 2 Linear trends, annual and semiannual amplitudes, and their associated uncertainties for both anthropogenic water consumption data (postsubtraction of energy sector water consumption) and surface water and groundwater data (postsubtraction of energy sector water consumption).

	Linear trend [mm/yr]	**Annual amplitude [mm]**	**Semiannual amplitude[mm]**
Anthropogenic water consumption	-3.35±0.14	5.43±1.16	1.08±1.16
Surface water and Groundwater change	-4.35±0.13	12.20±1.11	0.23±1.11

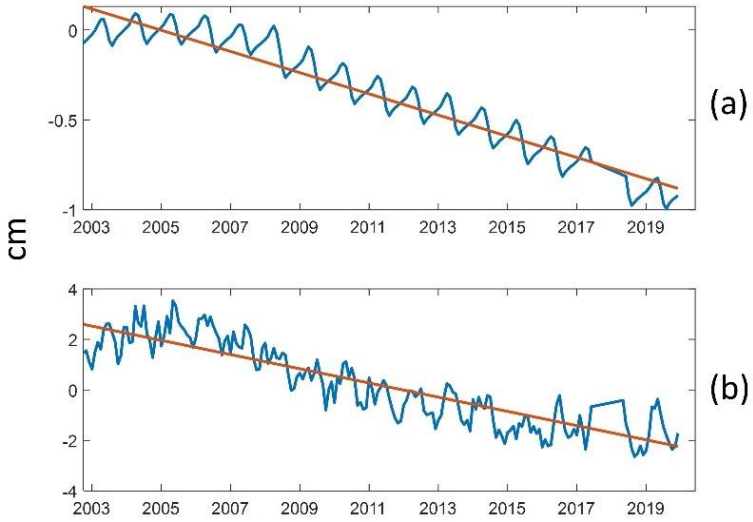

Fig. 9 (a) Anthropogenic influences on ground water derived from the WGHM hydrological model and (b) anthropogenic influences on surface water. Both datasets share consistent temporal coverage spanning 2002.10–2019.12.

(with energy sector impacts excluded) tends to be -3.35 ± 0.14 mm/yr, accounting for 77 % of groundwater/surface water variations and 64 % of TWSC changes, which is consistent with findings from prior studies in regions experiencing significant human-induced hydrological modifications (Feng et al., 2013).

4.4. VALIDATION OF ANALYTICAL OUTCOMES

Given Iran's significant reliance on groundwater extraction (Safdari, 2022), agricultural irrigation emerged as the dominant driver of human water use in Iran after water consumption by the energy sector was excluded from the total anthropogenic water withdrawal data. Irrigation water is primarily lost through ET, with secondary partitioning into groundwater recharge and surface runoff. The anthropogenic impact on groundwater is quantified using net groundwater abstraction data from the WGHM. This impact counterbalances the groundwater recharge contribution from ET losses. The residual anthropogenic influence on surface water atributable to irrigation losses positively correlates with ET fluxes. The anthropogenic effects on groundwater water are shown in Figure 9(a), and the anthropogenic effects on surface water are shown in Figure 9(b).

The sharp decrease in net groundwater abstraction since 2007, attributable to anthropogenic overabstraction, is shown in Figure 9(a). This trend corresponds closely with the progressive decrease in TWSC observed after 2007 in Figure 3, mutually reinforcing the identified depletion pattern.

As presented in Table 3, the linear decrease in groundwater storage in Iran attributable to anthropogenic influences is -0.59±0.02 cm/yr, with extraction rates significantly exceeding natural recharge. This persistent imbalance has induced land subsidence and associated geological consequences, ultimately causing irreversible hydrological impacts on local water resources. While abstracted groundwater is primarily utilized for agricultural irrigation with return to surface systems, surface water is depleted via evapotranspiration and runoff. The cumulative ET and its linear trend, which are calculated using the GLDAS hydrological model, are shown in Figure 10.

As shown in Figure 10, the linear trend of ET is -1.92±0.22 mm/yr, with annual and semiannual amplitudes of 12.59±1.52 mm and -1.62±1.52 mm, respectively. The strong correlation (r=0.73) with the anthropogenic surface water impact series confirms the dominance of agricultural irrigation on TWS in Iran. Notably, the observed long-term decrease in ET

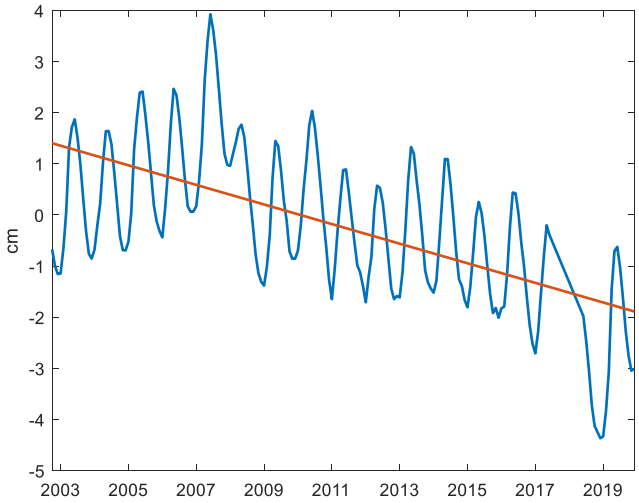

Fig. 10 The cumulative accumulation of latitude-weighted ET derived from GLDAS-Noah.

is slightly smaller in magnitude than the reduction rate in agriculture-dominated surface water consumption. This divergence is attributable to four primary factors. First, nonhydrological mass variations in Iran (including coal mining, glacial ablation, seismic activity and tectonic deformation) are not fully considered in current models. These components were excluded from the analysis because of their relatively small magnitude compared with that of the dominant hydrological processes. Second, as quantified by the Institute for Regional Water Consumption Studies (International Journal of Health Sciences, 2004–2020), Iran's improved oil recovery relies primarily on conventional water flooding techniques (~85 % of operations), whereas hydraulic fracturing and other high water-intensity methods constitute secondary contributors. This methodological emphasis may introduce inaccuracies in quantifying the energy sector's water consumption, particularly regarding the comprehensive capture of high-water-intensity extraction processes. Third, the potential overestimation of agricultural irrigation impacts may arise from methodological limitations. Our classification framework attributes all anthropogenic TWS changes including urban water supply systems and land use alterations exclusively to agricultural irrigation. Finally, inherent model discrepancies between the GLDAS-Noah and WGHM introduce systematic biases. Structural differences in their parameterization schemes, particularly regarding soil moisture dynamics and vegetation–atmosphere interactions, may lead to the underestimation or overestimation of actual hydrological processes.

5. CONCLUSION

In this study, the spatiotemporal evolution of the TWSC in Iran from 2002.4–2023.12 was reconstructed through a comprehensive analysis of Mascon solutions and hydrological models. During 2002–2006, Iran exhibited a state of relative hydrological balance, with generally stable and gradually increasing terrestrial water storage (mean linear trend increase: 0.12 ± 0.13 cm/yr). This trend was driven primarily (>75 % contribution) by precipitation variability. Significant water accumulation occurred in the southwest (46°–52°E, 28°–34°N; linear trend increase >3 cm/yr) and northeast (56°–60°E, 34°–37°N; linear trend increase >3 cm/yr), whereas the amount of water in other regions remained stable. However, a significant decrease in terrestrial water storage emerged across multiple regions after 2007 (mean linear trend decrease: -0.52 ± 0.03 cm/yr), which was primarily attributed to anthropogenic pressures, particularly industrial and agricultural water use. Although extreme precipitation anomalies led to a transient recovery in water storage between 2018 and 2021, anthropogenic consumption subsequently drove water scarcity to critical levels. The excessive anthropogenic exploitation of groundwater is strongly evident in the southern piedmont of the Alborz Mountains (48°–52°E, 34°–37°N), where the linear trend in TWS exceeded -20 cm/yr. This depletion was particularly severe in the western Tehran Plain (51.2°–51.5°E, 35.5°–35.7°N). Similarly, a localized linear trend in TWS decreases surpassing -10 cm/yr was observed in the Rafsanjan Basin (54°–59°E, 29°–31°N). Anthropogenic factors accounted for 77 % of the combined groundwater and surface water losses after the effects of water consumption for oil extraction in the energy sector were isolated. Furthermore, irrigation-induced groundwater extraction, which subsequently flows to the surface and is lost via evapotranspiration, constituted 64 % of these total losses. This unsustainable water use pattern has critically exacerbated water scarcity.

FUNDING

This work was funded by the National Natural Science Foundation of China (42064001), the National Natural Science Foundation of China (42374017), Graduate Innovation Fund of East China University of Technology (YC2024-B205).

DATA AVAILABILITY STATEMENT

Data will be available on request.

ACKNOWLEDGMENTS

The authors express their deep gratitude to the funding agency for supporting this research. We appreciate the editors and the two anonymous reviewers for their valuable suggestions and advice.

CONFLICTS OF INTEREST

The authors declare that they have no conflicts of interest.

REFERENCES

Akhtar, F., Nawaz, R.A., Hafeez, M., Awan, U.K., Borgemeister, C. and Tischbein, B.: 2022, Evaluation of GRACE derived groundwater storage changes in different agro-ecological zones of the Indus Basin. J. Hydrol., 605, 9, 127369. DOI: 10.1016/j.jhydrol.2021.127369

Alghafli, K., Shi, X., Sloan, W., Shamsudduha, M., Tang, Q., Sefelnasr, A. and Ebraheem, A.A.: 2023, Groundwater recharge estimation using in-situ and GRACE observations in the eastern region of the United Arab Emirates. Sci. Total Environ., 867, B, 161489. DOI: 10.1016/j.scitotenv.2023.161489

Aslam, R.A., Shrestha, S., Usman, M.N., Khan, S.N., Ali, S., Sharif, M.S., Sarwar, M.W., Saddique, N., Sarwar, A., Ali, M.U. and Arshad, A.: 2022, Integrated SWAT-MODFLOW modeling-based groundwater adaptation policy guidelines for Lahorep Pakistan under projected climate change, and human development scenarios. Atmosphere, 13, 12, 2001. DOI: 10.3390/atmos13122001

Azar, M.K., Shami, S., Nilfouroushan, F., Salimi, M., Bolorfroshan, M.G. and Reshadi, M.A.M.: 2022, Integrated analysis of Hashtgerd plain deformation, using Sentinel-1 SAR, geological and hydrological data. Sci. Rep., 12, 1. DOI: 10.1038/s41598-022-25659-4

Bhattarai, N., Pollack, A., Lobell, D.B. et al.: 2021, The impact of groundwater depletion on agricultural production in India. Environ. Res. Lett., 16, 8, 13 pp. DOI: 10.1088/1748-9326/ac10de

Boshnakov, G.N.: 2016, Introduction to time series analysis and forecasting, 2nd Edition. Wiley Series in Probability and Statistics.

Cao, Y., Nan, Z. and Cheng, G.: 2015, GRACE gravity satellite observations of terrestrial water storage changes for drought characterization in the arid land of Northwestern China. Remote Sens., 7, 1, 1021–1047. DOI: 10.3390/rs70101021

Long, D., Pan, Y., Zhou, J., Chen, Y., Hou, X., Hong, Y., Scanlon, B.R. and Longueyergne, L.: 2017, Global analysis of spatiotemporal variability in merged total water storage changes using multiple GRACE products and global hydrological models. Remote Sens. Environ, 192, 198–216. DOI: 10.1016/j.rse.2017.02.011

Eamus, D., Zolfaghar, S., Villalobos-Vega, R., Cleverly, J. and Huete, A.: 2015, Groundwater-dependent ecosystems: recent insights from satellite and field-based studies. Hydrol. Earth Syst. Sci., 19, 10, 4229–4256. DOI: 10.5194/hess-19-4229-2015

Ehsa, M., Shabbir, H., Al-Quraishi, A.M.F., Al-Ansari, N., Ahmad, Z., Abdelrahman, K., Sohail, M.T., Manzoor, Z., Shafi, A. and Elbeltagi, A.: 2024, Groundwater delineation for sustainable improvement and development aided by GIS, AHP, and MIF techniques. Appl. Water Sci., 14, 2, 21 pp. DOI: 10.1007/s13201-023-02065-3

Ellison, D., Pokorny, J. and Wild, M.: 2024, Even cooler insights: On the power of forests to (water the Earth and) cool the planet. Glob. Chang Biol., 30, 2, pp. 20. DOI: 10.1111/gcb.17195

Feng, W., Zhong, M., Lemoine, J., Biancale, R., Hsu, H. and Xia, J.: 2013, Evaluation of groundwater depletion in North China using the gravity recovery and climate experiment (GRACE) data and ground-based measurements. Water Resour. Res., 49, 4, 2110–2118. DOI: 10.1002/wrcr.20192

Hosseini-Moghari, S., Araghinejad, S., Ebrahimi, K., Tang, Q. and Aghakouchak, A.: 2020, Using GRACE satellite observations for separating meteorological variability from anthropogenic impacts on water availability. Sci. Rep., 10, 1, 12 pp. DOI: 10.1038/s41598-020-71837-7

Liu, M., Pei, H. and Shen, Y.: 2022, Evaluating dynamics of GRACE groundwater and its drought potential in Taihang Mountain Region, China. J. Hydrol., 612, 128156. DOI: 10.1016/j.jhydrol.2022.128156

Loomis, B.D., Rachlin, K.E., Wiese, D.N., Landerer, F.W. and Luthcke, S.B.: 2020, Replacing GRACE/GRACE - FO C30 with satellite laser ranging: Impacts on Antarctic Ice Sheet mass change. Geophys. Res. Lett., 47, 3, 7 pp. DOI: 10.1029/2019GL085488

Luan, M.A., Guang-Cai, W., Zhe-Ming, S., Yu-Ying, G., Qing-Yu, X.U. and Xu-Juan, H.: 2016, Simulation of groundwater level recovery in abandoned mines, Fengfeng coalfield, China. J. Groundw. Sci. Eng., 4, 4, 344-353.

Ma, N., Szilagyi, J. and Zhang, Y.: 2021, Calibration-free complementary relationship estimates terrestrial egapotranspiration globally. Water Resour. Res., 57, 9, 27 pp. DOI: 10.1029/2021WR029691

Mcstraw, T.C., Pulla, S.T., Jones, N.L., Williams, G.P., David, C.H., Nelson, J.E. and Ames, D.P.: 2022, An open-source wb application for regional analysis of GRACE groundwater data and engaging stakeholders in groundwater management. J. Am. Water Resour. Assoc., 58, 6, 1002–1016. DOI: 10.1111/1752-1688.12968

Metois, M., Benjelloun, M., Lasserre, C., Grandin, R., Barrier, L., Dushi, E. and Koci, R.: 2020, Subsidence associated with oil extraction, measured from time series analysis of Sentinel-1 data: case study of the Patos-Marinza oil field, Albania. Solid Earth, 11, 2, 363–378. DOI: 10.5194/se-11-363-2020

Mohasseb, H.A., Shen, W. and Jiao, J.: 2024, Monsoon-based linear regression analysis for filling data gaps in gravity recovery and climate experiment satellite observations. Remote Sens., 16, 8, 25 pp. DOI: 10.3390/rs16081424

Ohmer, M., Liesch, T. and Wunsch, A.: 2022, Spatiotemporal optimization of groundwater monitoring networks using data-driven sparse sensing methods. Hydrol. Earth Syst. Sci., 26, 15, 4033–4053. DOI: 10.5194/hess-26-4033-2022

Panahi, D.M., Kalantari, Z., Ghajarnia, N., Seifollahi-Aghmiuni, S. and Destouni, G.: 2020, Variability and change in the hydro-climate and water resources of Iran over a recent 30-year period. Sci. Rep., 10, 1, 9 pp. DOI: 10.48550/arXiv.2302.11245

Pelliccia, L., Lorenz, M., Heyde, C., Kaluschke, M., Klimant, P., Knopp, S., Scheifenbaum, S., Rotsch, C., Weller, R., Werner, M., Zachmann, G., Zajonz, D. and Hammer, N.: 2020, A cadaver-based biomechanical model of acetabulum reaming for surgical virtual reality training simulators. Sci. Rep., 10, 1, 12 pp. DOI: 10.1038/s41598-020-71499-5

Safdari, Z.: 2022, Estimation of groundwater depletion in Iran´s catchments using well data. Water, 14, 1, 131 pp. DOI: 10.3390/w14010131

Safdari, Z., Nahavandchi, H. and Joodaki, G.: 2022a, Estimation of groundwater depletion in Iran's catchments using well data. Water, 14, 1, 19 pp.

Scanlon, B.R., Zhang, Z., Save, H., Sun, A.Y., Schmied, H.M., van Beek, L.P.H., Wiese, D.N., Wada, Y., Di L., Reedy, R.C., Longuevergne, L., Doll, P. and Bierkens, M.F.P.: 2018, Global models underestimate large decadal declining and rising water storage trends relative to GRACE satellite data.hi. Proc. Natl. Acad. Sci. USA, 115, 6, E1080–E1089. DOI: 10.1073/pnas.1704665115

Shi, T., Guo, J., Yan, H., Chang, X., Ji, B. and Liu, X.: 2022, Assessing height variations in Qinghai-Tibet Plateau from time-varying gravity data and hydrological model. Remote Sens., 14, 19, 20 pp. DOI: 10.3390/rs14194707

Su, Y., Guo, B., Zhou, Z., Zhog, Y. and Min, L.: 2020, Spatio-temporal variations in groundwater revealed by GRACE and its driving factors in the Huang-Huai-Hai plain, China. Sensors, 20, 3, 17 pp. DOI: 10.3390/s20030922

Sun, P., Li, M., Guo, C. and Wei, D.: 2024, The relationship between GRACE gravity and the seismic b-value: a case study of the Northern Chile Triple Junction (25° S-40° S). Geophys. J. Int., 237, 3, 1575–1608. DOI: 10.1093/gji/ggae116

Sun, Z., Zhu, X., Pan, Y., Zhang, J. and Liu, X.: 2018, Drought evaluation using the GRACE terrestrial water storage deficit over the Yangtze River Basin, China. Sci. Total Environ., 634, 727–738. DOI: 10.1016/j.scitotenv.2018.03.292

Taheri, M., Dolatabadi, N., Nasseri, M., Zahraie, B., Amini, Y. and Schoups, G.: 2020, Localized linear regression methods for estimating monthly precipitation grids using elevation, rain gauge, and TRMM data. Theor. Appl. Climatol., 142, 1-2, 623–641. DOI: 10.1007/s00704-020-03320-2

Tu, J., Gu, D., Wu, Y., Yi, D. and Wang, J.: 2012, Phase error modeling and its impact on precise orbit determination of GRACE satellites. Math. Probl. Eng., 2012, 1, 710586. DOI: 10.1155/2012/710586

Voss, K.A., Famiglietti, J.S., Lo, M., de Linage, C., Rodell, M. and Swenson, S.C.: 2013, Groundwater depletion in the Middle East from GRACE with implications for transboundary water management in the Tigris-Euphrates-Western Iran region. Water Resour. Res., 49, 2, 904–14. DOI: 10.1002/wrcr.20078

Wada, Y., van Beek, L.P.H., van Kempen, C.M., Reckman, J.W.T.M., Vasak, S. and Bierkens, M.F.P.: 2010, Global depletion of groundwater resources. Geophys. Res. Lett., 37, 20, L20402. DOI: 10.1029/2010GL044571

Wang, S., Cui, G., Li, X., Liu, Y., Li, X., Tong, S. and Zhang, M.: 2023, GRACE satellite-based analysis of spatiotemporal evolution and driving factors of groundwater storage in the black soil region of Northeast China. Remote Sens., 15, 3, 19. DOI: 10.3390/rs15030704

Wang, S., Zhou, F. and Russell, H.A.J.: 2017, Estimating snow mass and peak river flows for the Mackenzie River Basin using GRACE satellite observations. Remote Sens., 9, 3, 20 pp. DOI: 10.3390/rs9030256

Wang, X., Liu, L., Niu, Q., Li, H. and Xu, Z.: 2021, Multiple data products reveal long-term variation characteristics of terrestrial water storage and its dominant factors in data-scarce Alpine regions. Remote Sens., 13, 12, 22 pp. DOI: 10.3390/rs13122356

Xiao, R., He, X., Zhang, Y., Ferreira, V.G. and Cchang, L.: 2015, Monitoring groundwater variations from satellite gravimetry and hydrological models: A comparison with in - situ measurements in the Mid-Atlantic region of the United States. Remote Sens., 7, 1, 686–703. DOI: 10.3390/rs70100686

Xu, Y., Gong, H., Chen, B., Zhang, Q. and Li, Z.: 2021, Long-term and seasonal variation in groundwater storage in the North China Plain based on GRACE. Int. J. Appl. Earth Obs. Geoinf., 104, 3, 10256016. DOI: 10.1016/j.jag.2021.102560

Yang, X., Wang, N., Liang, Q., Chen, A. and Wu, Y.: 2021, Impacts of human activities on the variations in terrestrial water storage of the Aral Sea Basin. Remote Sens., 13, 15, 17 pp. DOI: 10.3390/rs13152923

Yeh, P.J.F., Swenson, S.C., Famiglietti, J.S. and Rodell, M.: 2006, Remote sensing of groundwater storage changes in Illinois using the Gravity Recovery and Climate Experiment (GRACE). Water Resour. Res., 42, 12, W12203.1-W12203.7. DOI: 10.1029/2006WR005374

Zaki, N.A., Haghighi, A.T., Rossi, P.M., Tourian, M.J., Bakhshaee, A. and Klove, B.: 2020, Evaluating impacts of idrigation and drought on river, groundwater and a terminal wetland in the Zayanderud Basin, Iran. Water, 12, 5, 15 pp. DOI: 10.3390/w12051302

Zhang, E., Yang, S. and Zhang, L.: 2024, General waveguide bend design based on cubic spline interpolation and inverse design. J. Lightwave Technol., 42, 13, 4614–4625. DOI: 10.1109/JLT.2024.3370675